第34卷 第2期 焊 接 学 报 Vol. 34 No. 2
2013年2月 TRANSACTIONS OF THE CHINA WELDING INSTITUTION February 2013

钛及钛合金X射线应力测试参数的选择

邓云华， 李晓延， 李庆庆， 芦 伟
(北京工业大学 材料科学与工程学院，北京 100124)

摘 要：针对钛及钛合金X射线应力测试中衍射峰强度低、峰形差、测试结果波动范围大和准确度低等问题，通过对标准零应力试样和标准应力试样的X射线应力测试，研究了钛及钛合金X射线应力测试中准直器直径、计数时间和计数次数变化对衍射峰强度、净峰强度、半高宽、应力测试结果的影响规律，在此基础上确定了钛及钛合金X射线应力测试参数的选择方法，并对钛合金电子束焊接头的残余应力进行了测试. 结果表明，随着准直器直径增大和计数时间增长，衍射峰强度增大，衍射峰形改善，测试结果准确性提高；随着计数次数增加，衍射峰形改善，测试结果准确性提高；所确定的测试参数对钛合金电子束焊接头残余应力测试的结果满足相关标准要求.

关键词：钛合金； X射线应力测试； 测试参数
中图分类号：TG404 **文献标识码**：A **文章编号**：0253－360X(2013)02－0031－04

邓云华

0 序 言

钛及钛合金材料具有质量轻、强度高、比强度大、耐腐蚀性等优点，广泛地应用于航空航天和石化等领域[1－3]. 钛及钛合金材料在焊接等加工制造中不可避免地会产生残余应力，残余应力对于钛合金结构的疲劳性能和应力腐蚀性能方面有着重要影响. 无损地准确测定钛及钛合金材料的残余应力对于评定钛及钛合金制品的疲劳性能、抗应力腐蚀能力和服役寿命等具有重要意义.

X射线应力测试是当前广泛采用的一种无损应力测试方法. 在X射线应力测试中，选定测试靶材和衍射晶面后，衍射峰强度、净峰强度、半高宽和衍射峰形是影响测试结果准确度的主要因素. 国内外已有研究结果表明，衍射峰强度和净峰强度越高，测试结果精度越高；半高宽越大，随机误差越大，测试结果准确度越低；衍射峰形越平滑，测试结果准确度越高[4,5]. 钛及钛合金材料中Ti原子对X射线的质量吸收系数大、荧光效应强和原子散射因子相对较小，在进行X射线衍射应力测试时，衍射峰强度和净峰强度低、背底强度大、峰形差，进而导致测试结果波动范围大、准确度低[6,7]. 准确地测定钛及钛合金材料的残余应力值，需要解决上述影响测试准确度的相关问题，选择合适的X射线应力测试参数是解决这一问题的途径.

文中通过对标准零应力试样和标准应力试样的X射线应力测试，研究了钛及钛合金X射线衍射应力测试准直器直径、计数时间和计数次数变化对衍射峰强度和净峰强度、衍射峰形以及半高宽的影响规律，在此基础上分析了钛及钛合金X射线应力测试准直器直径、计数时间和计数次数变化对应力测试结果的影响规律，最终给出了钛及钛合金残余应力X射线衍射应力测试参数的选择方法，并对钛合金电子束焊接头的残余应力进行了测试.

1 试验方法

试验设备型号为加拿大PROTO公司iXRD应力分析仪. 标准零应力试样材料为纯钛，标准应力试样材料为Ti6Al4V. 标准零应力试样和标准应力试样的相关X射线应力测试参数如表1所示.

表1 标准零应力和标准应力试样X射线应力测试相关参数

Table 1 X-ray stress measurement parameters of free stress standard sample and high stress standard sample

试样	X射线	衍射晶面 {*hkl*}	衍射角 2θ/(°)	X射线弹性常数 $1/2S_2/10^{-6}$ MPa	标准应力值 σ_s/MPa
标准零应力	Cu-K_α	{213}	139	11.887 8	0±14
标准应力	Cu-K_α	{213}	142	11.887 8	－662±35

收稿日期：2011－12－29
基金项目：国家自然科学基金重点资助项目(50935008)

在 X 射线衍射应力测试中除了表 1 所示的参数之外还需要选择 X 射线入射线与试样表面法线夹角 ψ_0 位置、摇摆角度、准直器直径、计数时间和计数次数. 试验中 ψ_0 位置为 30°,24.8°,19.29°,11.48°,5.55°,0°,−5.55°,−11.48°,−19.29°,−24.8°,−30°. 摇摆角度对 X 射线应力测试的影响已有较多研究[6-8],增加摇摆角度可以提高衍射峰强度,改善峰形,尤其在粗晶粒材料中增大摇摆角度可以获得良好的测试结果,考虑钛及钛合金衍射峰强度低,摇摆角度选择为 3°. 准直器直径分别选择 1,2,3,4 mm,计数时间分别选择 1,2,4 s,计数次数分别选择 5 次,15 次,25 次,以此考察准直器直径、计数时间和计数次数变化对测试结果的影响. 依据标准 ASTM E915-10 和 BS EN 15305:2008 每种测试参数连续进行 5 次测量. 将每一种参数下测试的应力结果看作反映被测试样应力值的一个样本.

焊接接头材料为 TC4 合金,焊件尺寸为 240 mm × 150 mm × 12.5 mm. 电子束穿透焊,焊后电子束修饰. 残余应力 X 射线测试前使用丙酮、酒精溶液清洗被测焊件表面.

2 试验结果与讨论

2.1 测试参数对衍射峰强度和净峰强度的影响

测试参数对衍射峰强度和净峰强度的影响可通过分析测试参数对衍射峰最大相对强度 I_{max} 和峰背比的影响来考查. 衍射峰强度恒定的情况下,峰背比越大,净峰强度越大. 测试参数对衍射峰强度和峰背比影响规律如图 1 和图 2 所示.

由图 1 和图 2 可以看出标准零应力试样和标准应力试样反映出的准直器直径、计数时间和计数次数对衍射峰强度和峰背比的影响规律一致. 图 1 表明,衍射峰强度主要取决于准直器直径和计数时间;准直器直径越大,衍射峰强度越大;准直器直径不变,计数时间越长,衍射峰强度越大;当准直器直径和计数时间不变,计数次数从 5 次增加到 25 次时,衍射峰强度略有增加,但是变化不显著. 图 2 表明,峰背比主要取决于准直器直径和计数时间;准直器直径越大,峰背比越高;准直器不变,计数时间越长,峰背比增大,但是增大的趋势不如准直器直径增加影响的大;当准直器直径和计数时间不变,计数次数从 5 次增加到 25 次时,峰背比有减小的趋势.

从图 1,图 2 表现出来的准直器直径、计数时间和计数次数对衍射峰强度和峰背比的影响规律可以看出,为了获得高的衍射峰强度并在得到较高衍射峰强度的同时获得大的净峰强度,需要选择较大的

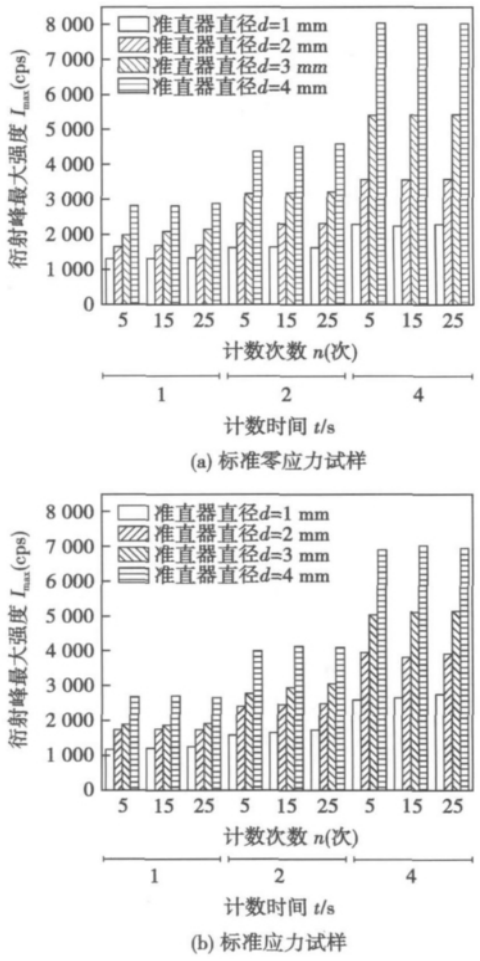

图 1 测试参数对衍射峰强度的影响

Fig. 1 Effects of measurement parameters on intensity of X-ray diffraction peak

准直器直径和较长的计数时间,当准直器直径和计数时间不变时,计数次数的增加会使衍射峰强度略有增加,但是会使峰背比稍有减小,因此综合衍射峰强度和峰背比两个因素,当准直器直径和计数时间不变时,计数次数对净峰强度的影响可以忽略不计.

2.2 测试参数对衍射峰形的影响

图 3 给出了标准零应力试样部分准直器直径、计数时间和计数次数均为 5 次时 X 射线应力测试的衍射峰形,可以看出准直器直径和计数时间的增加使衍射峰形平滑,在准直器直径和计数时间恒定的情况下,增加计数次数,衍射峰更加平滑.

2.3 测试参数对半高宽的影响

测试参数对半高宽的影响如图 4 所示,可以看出在对零应力和标准应力试样进行 X 射线应力测试时,准直器直径、计数时间、计数次数对衍射峰半高宽的影响规律基本一致. 准直器直径是影响半高宽变化的主要参数,准直器直径增加,半高宽增加. 图 4b 标准应力试样反映出的规律与标准零应力试

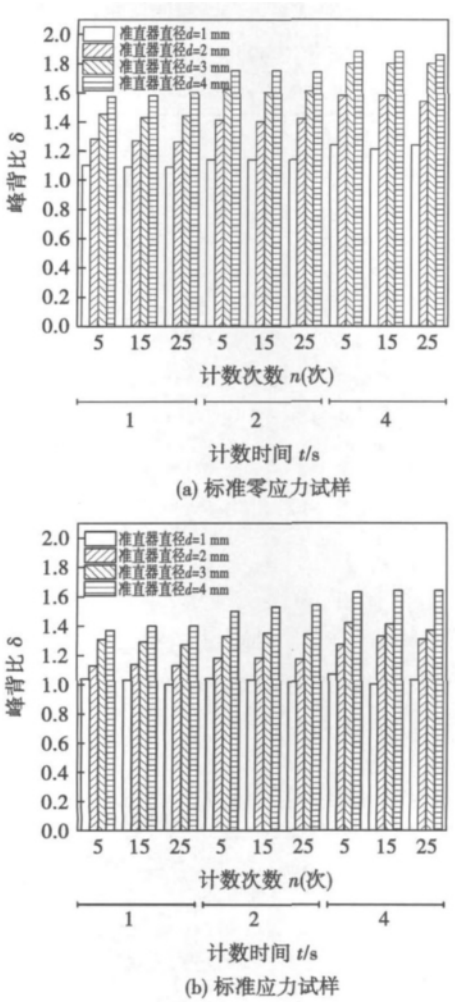

图 2　测试参数对峰背比的影响

Fig. 2　Effects of measurement parameters on peak-to-background ratio

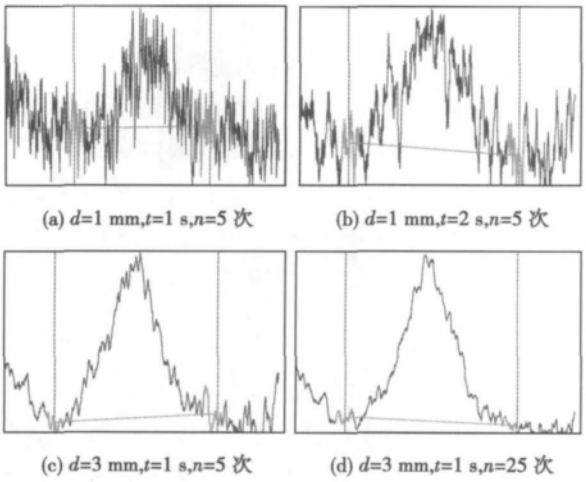

图 3　测试参数对衍射峰形的影响

Fig. 3　Effects of measurement parameters on X-ray diffraction profile

样一致,但标准应力试样半高宽值整体上比标准零应力试样大,原因在于标准应力试样中由于合金元素的添加,衍射峰会产生宽化.

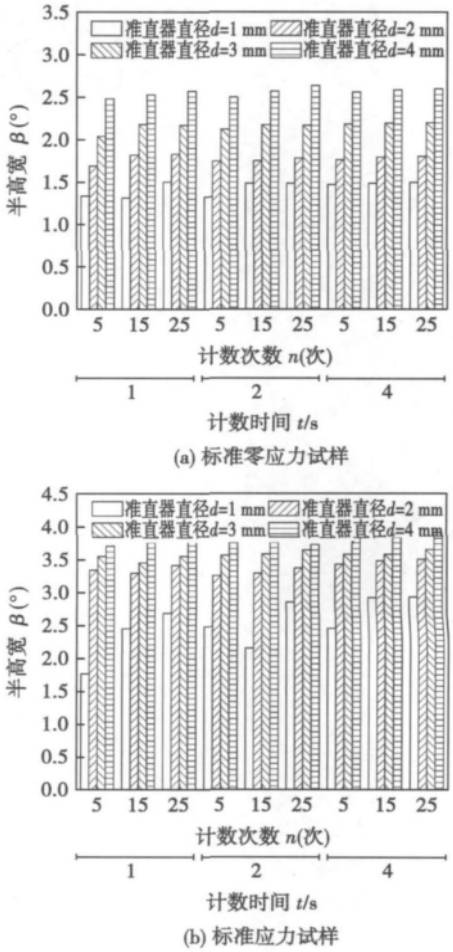

图 4　测试参数对半高宽的影响

Fig. 4　Effects of measurement parameters on full width at half maximum

2.4　测试参数对应力测试结果的影响

2.4.1　X 射线应力结果的评定

以测试样本均值和样本的 95% 置信区间作为评价 X 射线应力测试结果准确度的指标. 若测试样本均值在标准应力值范围之内,且 95% 置信区间 $[a,b]$ 长度 $l(l=(b-a)\ \mathrm{MPa})$ 不大于 20 MPa,则认为测试结果可信度高,此时所选择的测试参数能获得准确的应力测试结果.

2.4.2　测试参数对 X 射线应力测试结果的影响

满足 2.4.1 部分所要求条件的测试结果及相应测试参数如表 2 所示.

由表 2 可知,对于钛及钛合金 X 射线应力测试时满足要求的参数选择组合是: 准直器直径 $d\geqslant 4$ mm,计数时间 $t\geqslant 2$ s,计数次数 $n\geqslant 15$ 次. 原因在于当选择这一测试参数组合可以获得较高的衍射峰强

表 2 应力测试满足条件的测试参数及结果

Table 2 X-ray stress measurement parameters and results of free stress standard sample

试样	测试参数			测试结果	
	准直器直径 d/mm	计数时间 t/s	计数次数 n(次)	均值 σ_m/MPa	95% 置信区 [a, b] /MPa
标准零应力	3	4	25	4.96	[-0.66, 10.59]
	4	1	5	-2.61	[-10.20, 4.97]
	4	1	15	3.79	[-3.61, 11.18]
	4	1	25	1.61	[-5.37, 8.58]
	4	2	5	1.13	[-6.36, 8.63]
	4	2	15	-1.00	[-6.28, 4.27]
	4	2	25	-2.17	[-8.59, 4.25]
	4	4	5	-3.47	[-11.42, 4.48]
	4	4	15	1.82	[-1.78, 5.43]
	4	4	25	-3.40	[-11.24, 4.44]
标准应力	4	2	15	-661.55	[-669.71, -653.38]
	4	2	25	-658.53	[-662.13, -654.93]
	4	4	15	-666.34	[-673.02, -659.66]
	4	4	25	-657.34	[-663.13, -651.54]

表 3 应力测试最小计数时间及测试结果

Table 3 Measurement result and shortest exposure time needed for stress measurement

试样	测试参数			测试结果	
	准直器直径 d/mm	计数时间 t/s	计数次数 n(次)	均值 σ_m/MPa	95% 置信区 [a, b] /MPa
标准零应力试样	1	12	20	2.35	[7.33, -2.62]
	2	8	20	1.00	[4.19, -2.20]
	3	5	20	3.45	[8.55, -1.64]
标准应力试样	1	12	20	-658.12	[-649.22, -668.02]
	2	8	20	-664.83	[-656.45, -673.21]
	3	5	20	-658.98	[-651.10, -666.86]

度和良好的衍射峰形，进而能准确地确定衍射角，得到准确的 X 射线应力测试结果. 准直器直径的增加也会带来半高宽的增大，但是由于衍射峰强度的增大和峰形的改善，半高宽增加对测试结果准确度的不利影响被削弱.

实际被测材料由于尺寸因素方面的限制，测试区域难以满足直径 4 mm 的要求，此时结合测试参数对衍射峰强度影响的分析结果可知，可选择小的准直器直径并通过延长计数时间来提高 X 射线衍射强度，获得良好的衍射峰形，进而获得准确地测试结果. 因此试验中进一步研究了当准直器直径小于 4 mm 时的计数时间和次数的选择要求. 此条件下所需要的最短计数时间及测试结果见表 3.

由表 3 可知，当准直器直径分别为 1，2，3 mm 时，对应计数时间分别大于等于 12，8，5 s 可以获得准确的应力测试结果. 但是较小准直器直径，需要选择长的计数时间和计数次数，测试效率低，所以实际测试参数的选择还需考虑测试效率，在测试对象满足使用大的准直器直径的时候可优先选择大的准直器直径以提高测试效率.

2.5 钛合金焊接接头残余应力测试结果与分析

钛合金电子束焊接头残余应力分布见图 5. 根据 BS EN 15305:2008 标准，按试验所选参数进行钛合金焊接接头残余应力 X 射线测试，其结果应满足以下要求. (1) 当 X 射线应力测试结果 $|\sigma| \geqslant 210.3$ MPa 时，测试结果的误差应满足 $|u(\sigma)| \leqslant 52.57$ MPa；(2) 当 X 射线应力测试结果 $|\sigma| < 210.3$ MPa 时，测试结果的误差应满足 $|u(\sigma)| \leqslant 16.82$ MPa 或者 $|u(\sigma)| \leqslant |\sigma|/4$.

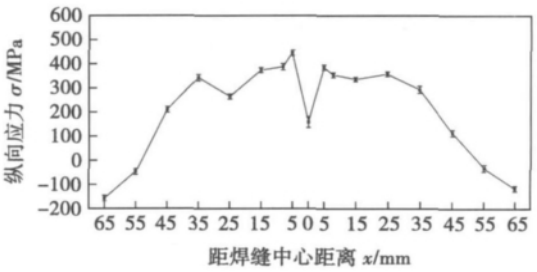

图 5 接头纵向残余应力测试结果沿横向的分布

Fig. 5 Distribution of longitudinal residual stresses along transverse direction

测试结果误差最大的测点在焊缝中心，误差为 ±22.74 MPa，其余各测点残余应力测试结果误差绝对值均小于 14.5 MPa，测试结果准确性满足标准要求. 焊缝中心处残余应力测试误差大的原因在于焊缝金属表面不平整，影响 X 射线衍射几何，进而带来较大的误差.

3 结 论

(1) 钛及钛合金材料 X 射线应力测试时，随着准直器直径增大和计数时间增长，衍射峰强度增大，衍射峰形改善，测试结果准确性提高. 当选择小的准直器直径时可以通过提高计数时间和计数次数来提高衍射峰强度，获取准确的应力值.

(2) 计数次数增加，衍射峰形改善，测试结果准

[下转第 39 页]

application anaysis of HVOF coating [J]. Journal of Hydroelectric Engineering, 2004, 23(5): 123 - 127.

[6] Wu Yuping, Lin Pinghua, Chu Chenglin. Cavitation erosion characteristics of a Fe-Cr-Si-B-Mn coating fabricated by high velocity oxy-fuel(HVOF) thermal spray [J]. Materials Letters, 2007, 61: 1867 - 1872.

[7] 李　刚. 纳米结构 WC-12Co 金属陶瓷涂层制备工艺及抗汽蚀机理的研究 [D]. 武汉: 武汉理工大学, 2007.

[8] 中国船舶重工集团公司第七二五研究所. GB/T 6383—2009 振动空蚀试验方法 [S]. 北京: 中国标准出版社, 2009.

[9] 吴玉萍, 林萍华, 王泽华, 等. HVOF 喷涂 Fe-Cr 基涂层中非晶与纳米晶形成的研究 [J]. 材料热处理学报, 2006, 27(2): 15 - 19.
Wu Yuping, Lin Pinghua, Wang Zehua, *et al*. Research of amorphous and nanocrystalline forbided by HVOF sprayed Fe-Cr coating [J]. Transactions of Materials and Heat Treatment, 2006, 27(2): 15 - 19.

[10] 吴玉萍, 林萍华, 曹　明, 等. Ni60 + TiC 等离子熔覆层的汽蚀特征 [J]. 材料热处理学报, 2007, 28(5): 128 - 133.
Wu Yuping, Lin Pinghua, Cao Ming, *et al*. Cavitation erosion characteristics of Ni60 + TiC plasma cladding layer coating [J]. Transactions of Materials and Heat Treatment, 2007, 28(5): 128 - 133.

[11] Chen Haosheng, Li Jiang. A ring area formed around the erosion pit on 1Cr18Ni9Ti stainless steel surface in incipient cavitation erosion [J]. Wear, 2009, 266: 884 - 887.

[12] 王荣克. 磨蚀泥沙启动装置的研制与泥沙特性对磨蚀影响的研究 [D]. 南京: 河海大学, 2007.

作者简介: 王　倩,女,1986 年出生,硕士. 主要从事材料表面的腐蚀与防护研究工作. 发表论文 2 篇. Email: happyqie521@163.com

通讯作者: 吴玉萍,女,教授,博士研究生导师. Email: wuyphhu@163.com

[上接第 34 页]

确性提高.

(3) 钛及钛合金材料 X 射线应力测试优化的参数选择方案是: 准直器直径分别为 1,2,3,4 mm 时,计数时间相应分别大于等于 12,8,5,2 s,计数次数大于等于 15 次.

(4) 所确定的测试参数对钛合金焊接接头残余应力的测试结果满足相关标准要求.

参考文献:

[1] Casavola C, Pappalettere C, Tattoli F. Experimental and numerical study of static and fatigue properties of titanium alloy welded joints [J]. Mechanics of Materials, 2009, 41: 231 - 243.

[2] 王桂生, 田荣璋. 钛的应用技术 [M]. 长沙: 中南大学出版社, 2007.

[3] Tsay L W, Tsay C Y. The effect of microstructures on the fatigue crack growth in Ti-6AI-4V laser welds [J]. International Journal of Fatigue, 1997, 19(10): 713 - 720.

[4] 吕克茂. 残余应力测定的基本知识—第四讲 X 射线衍射应力测定方法(二) [J]. 理化检验: 物理分册, 2007, 43(8): 428 - 432.
Lü Kemao. Basic knowledge of residual stress determination-lecture No. 4 stress determination method by X-ray(Ⅱ) [J]. Physical Testing and Chemical Analysis Part A: Physical Testing, 2007, 43(8): 428 - 432.

[5] Ruth E. Metals Handbook [M]. Ohio: Ohio American Society for Metals, 1986.

[6] Brouno G, Dunu B D. Surface and bulk residual stress in Ti6Al4V welded aerospace tanks [J]. Journal of Pressure Vessel Technology, 2004, 126(3): 284 - 292.

[7] Zhang Y L, Liu J Y, Wang J, *et al*. X-ray diffraction characteristics of five materials for stress measurement [J]. Journal of Strain Analysis for Engineering Design, 2010, 45(4): 319 - 328.

作者简介: 邓云华,男,1987 年出生,硕士研究生. 主要从事焊接残余应力 X 射线测试方面的研究工作. Email: yunhuadeng@emails.bjut.edu.cn

compounds started to react with Cu ball bonds to form Cu_3Sb. When the aging time is more than 49 hours at 250 ℃, Cu wire loop is broken and serious corrosion is found in Cu ball bond. Furthermore, Ag migration phenomenon occurs if the aging time is more than 24 hours at 250 ℃ or 4 hours at 300 ℃.

Key words: fine Cu wire; high temperature storage; IMC; reability; Ag migration

An ultrasonic SH-guided-wave transducer for ultrasonic imaging and testing of plate with welded structure ZHU Xinjie, CHEN Yifang, HAN Zandong, DU Dong (Key Laboratory for Advanced Materials Processing Technology, Ministry of Education, Tsinghua University, Beijing 100084, China). pp 17 – 21

Abstract: The SH (shear horizontal) guided waves can be used to test and image in long distance for the larger-sized plate in welded structure. The performance of ultrasonic SH-guided-waves transducer is essential to imaging and testing larger-sized plate in welded structure. The dynamic analysis of SH guided wave in plate and half-wave propagation conditions was carried out. The reasonable wedge angle, the frequency, size of the piezoelectric wafer for SH-guided-waves transducer and other important parameters were designed. The steps such as adding the front lining, removing the back lining, setting the jagged slot on front wedge and so on, have reduced the internal echo interference in SH-guided-waves transducer, which improves the testing sensitivity and simplifies the transducer structure. The results shows that the developed SH-guided-waves transducer has the better testing ability and can be used in imaging and testing complex T-butt type welded structure. The image can characterize the defects, whose size is close to the guided wave length in the welded structure. The proposed research provides the foundation for the imaging and testing of larger-sized plate with welded structure.

Key words: ultrasonic; shear horizontal-guided-wave transducer; welded structure

Effect rule of torch angle change on weld formation of keyhole plasma arc welding JIANG Fan, CHEN Shujun, WANG Long, YU Yang (College of Mechanical Engineering and Applied Electronics Technology, Beijing University of Technology, Beijing 100124, China). pp 22 – 26

Abstract: By taking 5 mm thick 5A06 aluminum-magnesium alloy as the main researching object, the front and back weld width as the formation parameter, the significance of torch angle to weld formation was studied by the orthogonal experiment, the effect of change of torch angle on weld formation was studied from the point of energy transfer. The result shows that the influence of the torch angle on welding formation is between current and plasma gas flow rate. There is largest front weld width when the torch is perpendicular to the test plate. The back weld width will be larger with the torch angle increasing. It indicates the energy density on the front surface, the relative position of the highest temperature section and the widest molten section will be changed by torch angle change. The effect on the back weld width may be caused by the interaction of sectional heat source deviation of different thickness direction and the delay of heat transfer.

Key words: keyhole plasma arc welding; torch travelling angle; weld formation; orthogonal experiment

Statistic analysis on spatter characteristics in high power CO_2 laser and fiber laser welding of thin sheet aluminum alloy CAI Hua, XIAO Rongshi (Institute of Laser Engineering, Beijing University of Technology, Beijing 100124, China). pp 27 – 30

Abstract: Spatters in laser penetration welding of aluminum alloys affects the process stability and reflects the laser welding process to a certain degree. The spatter characteristics in CO_2 laser and fiber welding of 6061-T6 aluminum alloy were investigated, and the reasons for the difference in spatter characteristics were discussed. Dynamic behavior of spatters was recorded in real-time by a high-speed camera. The spatter particles were captured and their sizes were measured experimentally. Probability density functions (PDFs) about the spatter velocity and size were fitted by Ordinary Least Squares (OLS) method in X^2 test. The result indicates that the spatter speed follows Gaussian distribution and the particle size follows lognormal distribution in both cases. However, the statistical speed of spatters is faster in fiber laser welding, which indicates that more attention should be paid to protect the focusing system. Moreover, the statistical diameters of the spatter particles are smaller and PDFs of the particle size is more fit with Lognormal distribution in fiber laser welding, which means that fiber laser welding process is more stable than CO_2 laser welding process.

Key words: thin sheet aluminum alloy; high power laser welding; spatter characterization; statistic analysis

Selection method of X-ray diffraction stress measurement parameters for titanium and titanium alloy DENG Yunhua, LI Xiaoyan, LI Qingqing, LU Wei (School of Materials Science and Engineering, Beijing University of Technology, Beijing 100124, China). pp 31 – 34, 39

Abstract: Considering the low intensity of diffraction peak, bad diffraction profile, wide fluctuation range and low accuracy of the stress measurement results for titanium and titanium alloy, the effects of aperture diameter, exposure time, and exposure number on the intensity of X-ray diffraction peak, net intensity, full width at half maximum, and the stress measurement results were investigated through the X-ray stress measurement of free stress standard sample and high stress standard sample. On this basis, the selection method of X-ray diffraction stress measurement parameters for titanium and titanium alloy was decided and used in measuring the residual stresses in TC4 welded joint. Results show that with the increase of aperture diameter and exposure time, the intensity of X-ray diffraction peak increases, both the diffraction profile and the accuracy of the test results are improved. What's more, with the increase of exposure number, the diffraction profile and the accuracy of the test results are also improved. The measurement results of residual stresses in TC4 welded joint meet the requirements of the related standards.

Key words: titanium alloy; X-ray stress measurement;

measurement parameter

Analysis of silt cavitation erosion resistance of Cr_3C_2/NiCr coating prepared by high velocity oxy-fuel thermal spraying

WANG Qian, WU Yuping, LI Gaiye, GUO Wenmin (College of Mechanics and Materials, Hehai University, Nanjing 210098, China). pp 35 – 39

Abstract: A Cr_3C_2/NiCr coating was prepared on 1Cr18Ni9Ti stainless steel by high velocity oxy-fuel (HVOF) thermal spraying. Phases and microstructures of the coating were analyzed by X-ray diffraction (XRD), transmission electron microscope (TEM) and scanning election microscopy (SEM), respectively. The cavitation erosion resistance and silt erosion resistance of the coating were evaluated under two experimental conditions (fresh water and water contained fine silt), and compared with hydro machine material 1Cr18Ni9Ti stainless steel. The result shows that the coating shows a layered structure and contains un-melted particles and some pores. The phases of the coating are composed of Cr_3C_2, Cr_7C_3, $Cr_{23}C_6$ and NiCr. The 1Cr18Ni9Ti stainless steel produces the work hardening, which results in the resistance to cavitation erosion. The Cr_3C_2/NiCr coating exhibits significantly higher microhardness than 1Cr18Ni9Ti stainless steel, which leads to the resistance to silt erosion of the coating. The mass loss of the coating usually happens at the edges of the pores while the cavitation damage of the 1Cr18Ni9Ti stainless steel happens at the grain boundary and twin boundary.

Key words: high velocity oxy-fuel; silt erosion; Cr_3C_2/NiCr coating; 1Cr18Ni9Ti stainless steel

Effect of process parameters on porosity formation ratio in dual-beam laser welding of aluminum alloys with filler wire

LEI Zhenglong[1], LI Ying[1], CHEN Yanbin[1], SUN Zhongshao[2], ZHANG Yikun[2] (1. State Key Laboratory of Advanced Welding and Joining, Harbin Institute of Technology, Harbin 150001, China; 2. Capital Aerospace Machinery Company, Beijing 100076, China). pp 40 – 44

Abstract: The characterizations of porosity in dual-beam laser welding with filler wire of LF6 aluminum alloys were studied. Compared with the single beam laser welding with filler wire and the dual-beam laser self-fusible welding, the dual-beam laser welding with filler wire can restrain the porosity formation. Especially, the dual-beam laser welding with parallel arrangement has a better effect on inhibition of porosity. Furthermore, the effects of shielding gas component and laser energy on porosity formation ratio were analyzed. The results show that, when the helium is used as the shielding gas, the area of plasma decreases as well as the shielding effect of the plasma on laser deceases, and the welding process become more stable. At the same time, the laser power must be proper, and both too high and too low laser power make the porosity formation ratio enlarged.

Key words: dual-beam laser welding with wire filling; porosity; process parameter; aluminum alloys

Rapidly tiny resistance welding of $Fe_{78}Si_9B_{13}$ amorphous foils

LING Shiquan, WU Xiaoyu, XU Bin, LUO Feng (ShenZhen Key Laboratory of Advanced Manufacturing Technology for Mold&Die, ShenZhen University, Shenzhen 518060, China). pp 45 – 48

Abstract: Rapidly tiny resistance welding of $Fe_{78}Si_9B_{13}$ amorphous foils with the thickness of 30 μm was conducted by using an inversion DC resistance welding machine. The welding parameters which affect the property of amorphous foils were discussed. The high quality joints were got without welding defects and welding parameters are as follow: 2 ms welding time, 0.2 V welding voltage and 56 N welding force. The average shear strength of the joint reaches 632 MPa. XRD test shows that the joint is amorphous structure. The cooling rate in the joint reaches 7.9×10^6 K/s, which is calculated by nucleation kinetics model, and obviously higher than the critical cooling rate of amorphous $Fe_{78}Si_9B_{13}$, and effectively prevents the crystallization of weld region. The study in this paper has high practical value in engineering.

Key words: Fe-based amorphous foil; resistance welding; joint properties; nucleation kinetics

Evaluation of stress corrosion of duplex stainless steel overlay

WANG Jing[1], ZHANG Yiliang[1], QIU Fei[1], WU Daowen[2] (1. Department of Mechanical Engineering & Applied Electronics Technology, Beijing University of Technology, Beijing 100124, China; 2. Luoyang Shuangrui Special Equipment Co., Ltd, Luoyang 471039, China). pp 49 – 53

Abstract: In order to prevent stress corrosion in petrochemical facilities, 2205 duplex stainless steel was deposited on the surface contacted with the corrosive media in projects. In order to explore the application scope and feasibility of the solution, two welding processes (automatic welding and manual welding), three kinds of common corrosion environment (saturated hydrogen sulfide, magnesium chloride, calcium chloride) were used to evaluate its stress corrosion comprehensively at the constant tensile load based on the microanalysis of fracture, and the mathematical model of stress-life was established based on the experimental results. The results indicate that the constant tensile load threshold is 0.45 R_{eL} for automatic welding and 0.4 R_{eL} for manual welding in saturated H_2S environment, and there is an error of 17% between them. All the samples are good after 96 hours in 0.9 R_{eL} stress test with the calcium chloride environment, which shows the excellent resistance to chloride stress corrosion. But the coating cannot be used in boiling magnesium chloride environment.

Key words: duplex stainless steel; surfacing; stress corrosion

Effect of single-component activating flux on weld morphologies in A-TIG welding of aluminum alloy

YAN Keng, GAO Lihua, YANG Gang, XIAO Hailin (Provincial Key Lab of Advanced Welding Technology, Jiangsu University of Science and Technology, Zhenjiang 212003, China). pp 54 – 57, 62

Abstract: A-TIG welding experiments of 6 mm 6061 aluminum alloy were carried out to investigate the effects of activating fluxes on weld appearance and macroscopic morphologies by using five kinds of single-component activating fluxes such as